1

A PREDICTIVE MODEL FOR WHISKER FORMATION BASED ON LOCAL MICROSTRUCTURE AND GRAIN BOUNDARY PROPERTIES

PYLIN SAROBOL

Sandia National Laboratories, Albuquerque, New Mexico, USA

YING WANG

School of Materials Engineering, Purdue University, West Lafayette, Indiana, USA

WEI-HSUN CHEN

School of Materials Engineering, Purdue University, West Lafayette, Indiana, USA; Cymer, Inc., San Diego, California, USA

AARON E. PEDIGO

Naval Surface Warfare Center, Crane Division, Crane, Indiana, USA

JOHN P. KOPPES

Alcoa-Howmet, Whitehall, Michigan, USA

JOHN E. BLENDELL AND CAROL A. HANDWERKER

School of Materials Engineering, Purdue University, West Lafayette, Indiana, USA

1.1 INTRODUCTION

For over 60 years, whiskers and hillocks have been recognized as local manifestations of stress relaxation in thin films: these “surface defects” grow spontaneously by mass transport to specific grain boundaries in the plane of the film, with whiskers becoming

Mitigating Tin Whisker Risks: Theory and Practice, First Edition.
Edited by Takahiko Kato, Carol A. Handwerker, and Jasbir Bath.

Companion website: www.wiley.com/go/Kato/TinWhiskerRisks

hillocks when grain boundary migration accompanies growth out of the plane of the film. Whisker formation is important for two reasons.

First, the risk to electronic system reliability is serious for whisker formation in Sn films: whiskers can sometimes grow to be millimeters long, causing short-circuiting between adjacent components. Second, isolating the mechanisms leading to whisker and hillock formation in one grain out of 10^3–10^5 film grains will inform us more broadly about the multiplicity of possible responses of thin films to stresses.

As a local phenomenon, whisker formation has been attributed in the past to specific inhomogeneity in either the film or the interfacial intermetallic microstructure, in stress, or in the anisotropic properties in the film. These inhomogeneities include

- grains above large Cu_6Sn_5 intermetallic particles [1, 2];
- grains covered by relatively weak oxide films [3];
- grains with larger out-of-plane elastic deformation than surrounding grains due to elastic anisotropy under plane strain conditions [4];
- a difference in the orientation-dependent yielding behavior of whisker grains and their neighboring grains [5, 6];
- shallow grains whose grain boundaries serve as sinks for atoms when surface diffusion necessary for diffusional creep is not active [7].

When the first three of these concepts were tested experimentally, these simple relationships were not observed. For example, Pei et al. [8] determined from electron backscatter diffraction (EBSD) and etching studies that whiskers were not associated with large underlying intermetallic particles. Moon et al. [9], Jadhav et al. [10], and A.E. Pedigo (unpublished research) determined through ultra-high vacuum (UHV) studies of sputtered films and through oxide removal in specific regions by focused ion beam (FIB) milling that whisker growth was unchanged when the native oxide layer was removed through sputtering and was not accelerated in regions without oxide.

From these and other experiments on the crystallography, texture, geometry, and strain in whisker and hillock grains relative to their surrounding microstructures, it is clear that models ascribing whisker formation and growth to a single cause are too simplistic: they do not capture all relevant aspects of why that particular grain was predisposed to become a whisker out of 10^3–10^5 grains in the film nor do they provide quantitative predictions of growth rates under a wide range of conditions.

Whisker nucleation and growth must be examined at the local level, taking into consideration the microstructure and properties of the film, specifically grain boundary structure, as well as crystallography, grain geometry, and the role of oxide films.

In this chapter, we review the characteristic properties of the local microstructure around whisker and hillock grains with the aim to further identify why these particular grains and locations became predisposed to forming whiskers and hillocks.

On the local level, we suggest that three factors play major roles in determining which surface grains will become whiskers or hillocks: the surface grain geometry, crystallographic orientation-dependent grain boundary properties, and the microstructure-dependent local elastic strain/strain energy density.

These effects have been identified through our recent model of whisker growth by grain boundary sliding limited creep (with and without coupling between grain boundary migration and shear stress), finite element analysis of a wide range of textured microstructures in Sn films, and recent experimental studies of microstructural evolution during intermetallic compound (IMC)-induced and thermal-cycling-induced stresses [11].

In addition, we have identified specific film microstructures and textures that are predicted to produce whisker-prone environments under specific stress conditions. By simulating the relationship between film texture (axis and strength) and the localization of the strain energy in the microstructure, a necessary condition for whisker formation is proposed: grains with locally high strain energy will become whiskers. Thus, measuring global film properties (crystallographic texture and strain energy density) may be a useful first step in identifying whisker-prone films, but is not sufficient in identifying which grain will form a surface defect.

Whisker growth will depend not only on local elastic strain energy density (ESED) but also grain geometry and the response of the grain boundaries surrounding the whisker grain to accretion-induced shear stresses.

1.2 CHARACTERISTICS OF WHISKER AND HILLOCK GROWTH FROM SURFACE GRAINS

Whiskers and hillocks typically grow from surface grains (Fig. 1.1) in fine-grained Sn and Sn-alloyed films in both isothermal (at room temperature or high temperature) and thermal cycling conditions. The origin of surface grains as nuclei for whiskers and hillocks have been much debated – whether surface grains were pre-existing

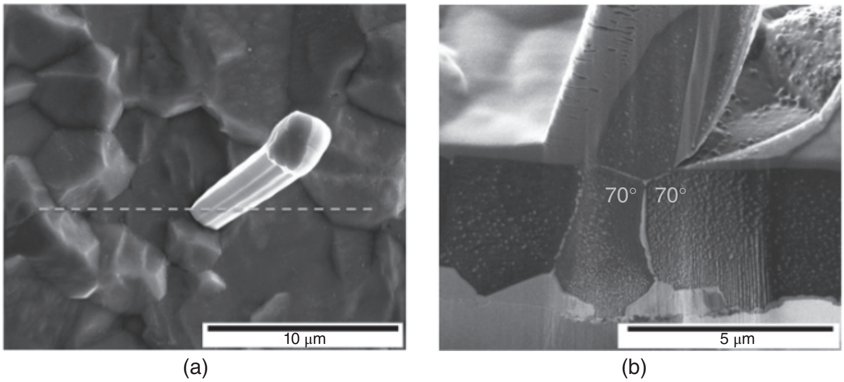

Figure 1.1 Whisker growing from surface grain. Image in (a) from secondary electron microscopy (SEM) shows a short whisker growing at an angle to the film top surface, while image in (b) from focused ion beam (FIB) cross section shows shallow grain boundaries (70° with respect to the film normal) at the whisker root. Source: Reprinted with permission from Elsevier © 2013 [12].

grains from the film deposition process [7, 13, 14], new grains that formed via surface recrystallization after the deposition process [7, 15, 16], or pre-existing grains whose topology changes as a result of grain growth in the film.

There is now direct evidence that whiskers and hillocks may form from either pre-existing or newly nucleated grains. Pei et al. [14] and Wang et al. [17] demonstrated that pre-existing grains could serve as nuclei for whiskers and hillocks for isothermal annealing (room temperature) and thermal cycling conditions, respectively.

Cross sections of whiskers formed under these conditions showed that the grain boundaries at the base of the whisker grain, that is, the "whisker root," are generally angled with respect to the film normal, creating shallow grains relative to the film thickness ("surface" grains) and that whiskers grew from grains with in-plane grain diameters typical of nonwhiskering grains in the film. In addition, surface grains that did not become whiskers or hillocks were also observed [12].

Shallow surface grains were observed by Sarobol et al. to form by recrystallization and grow into micron-sized whiskers and hillocks during thermal cycling of large-grained Sn-alloy films on Cu substrates, as seen in Figure 1.2 [18, 19]. New strain-free grains (low dislocation density) nucleated along pre-existing film grain boundaries and grew at the expense of highly deformed (high dislocation density) parent grains.

Hillocks are formed when growth out of the plane of the film is accompanied by grain boundary migration into the film, as seen in Figure 1.2c. Asymmetrical growth at the whisker root can lead to curved whiskers and hillocks, as shown in Figure 1.3 with a change in orientation of the whisker as it grows [8]. It is well known that the growth morphology for a given whisker and hillock may change over time, and since surface diffusion is suppressed by the presence of the surface oxide, the morphological changes over time are preserved in its surface shape [20].

1.2.1 Whisker Growth Model Based on Grain Boundary Sliding - Limited Creep

A growth model has been developed based on grain boundary faceting and grain boundary sliding limited Coble creep that explains the observed surface morphologies, the changing growth rate over time, and the dependence on grain geometry. In this model of whisker formation, two mechanisms are important: accretion of atoms by Coble creep on grain boundary planes normal to the growth direction (A_{accum}) inducing a grain boundary shear and grain boundary sliding on planes parallel to the direction of whisker growth (A_{slide}) with the grain boundary sliding coefficient determining whether accretion can lead to whisker formation.

The model accurately captures the importance of the geometry of surface grains – shallow grains on film surfaces whose depths are significantly less than their in-plane grain sizes.

A steady-state growth rate ($\Delta h/\Delta t$) of a whisker with constant radius can be calculated by

$$\frac{\Delta h}{\Delta t} = \frac{\Omega J A_{\text{accum}}}{\pi a^2} \tag{1.1}$$

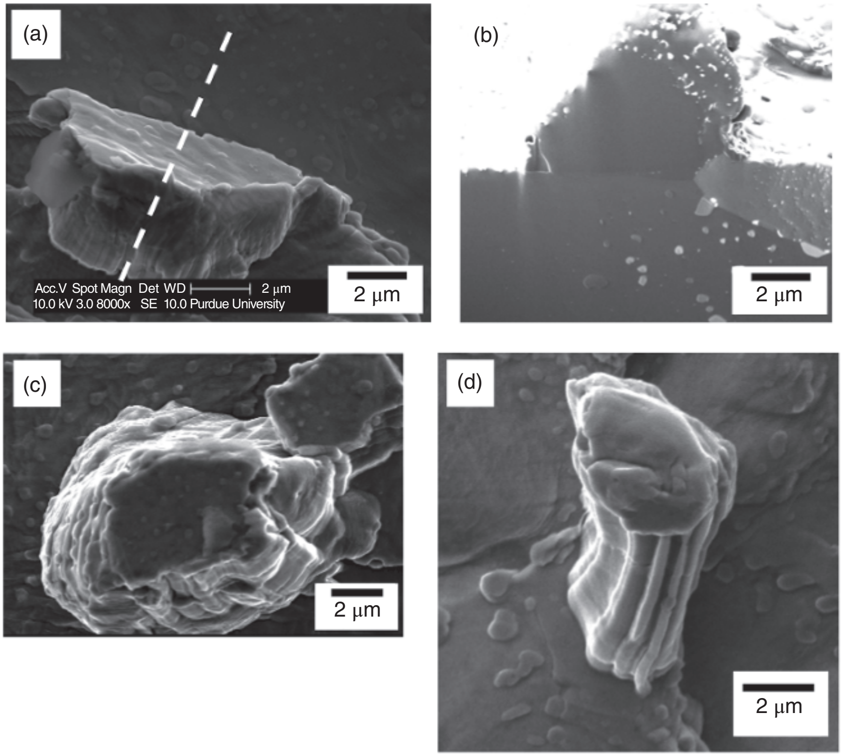

Figure 1.2 (a) Surface defect formed by recrystallization at a grain boundary, (b) with FIB cross section along the white dashed line in (a) showing shallow single-crystal grain with oblique grain boundaries, (c) representative hillock showing both surface uplift and grain boundary migration, and (d) representative whisker in thermally cycled solder film. Source: Reprinted with permission from Elsevier © 2013 [18].

where J is flux, A_{accum} is the area through which flux enters the surface grain and a is the surface grain radius. The flux, J, is estimated using a two-dimensional continuity equation, with $\nabla\sigma$ as the stress gradient that drives atomic flux toward the whisker base (σ_m at distance b away from the whisker center, which decreases toward the whisker edge). J and $\nabla\sigma$ are given by

$$J = \frac{D_{\text{eff}}\nabla\sigma}{RT} \tag{1.2}$$

$$\nabla^2\sigma = \frac{\partial^2\sigma}{\partial r^2} + \frac{1}{r}\frac{\partial\sigma}{\partial r} = 0 \tag{1.3}$$

$$\nabla\sigma|_{r=a} = \left.\frac{\partial\sigma}{\partial r}\right|_{r=a} = \frac{\Delta\sigma}{a\ln\left(\frac{b}{a}\right)} \tag{1.4}$$

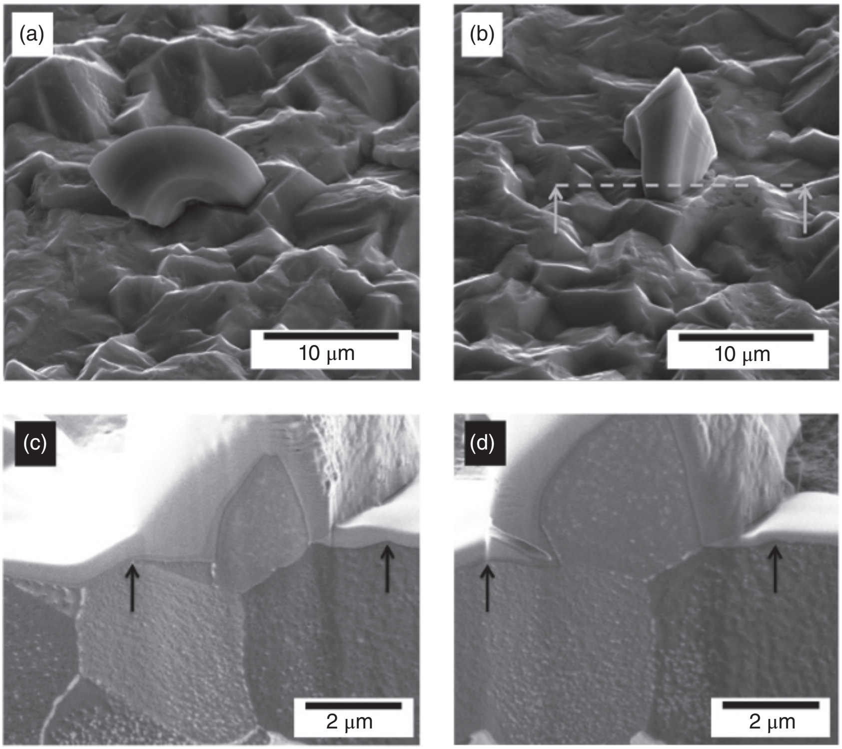

Figure 1.3 SEM images (a) and (b) from two different orientations of a curved whisker, which is decreasing in cross-sectional area as it grows. FIB images (c) and (d) show two successive cross sections of the whisker as oriented in (b), with the initial positions of the grain boundaries forming the whisker root indicated (black arrows). Source: Pei et al. [8].

The surface grain geometry is modeled as a stepped-cone shape with constant radius a and a cone angle of θ with effective accumulation area, $A_{\text{accum}} = \pi a^2$ and sliding area on the side, $A_{\text{slide}} = \frac{\pi a^2}{\tan\theta}$, as shown in Figure 1.4. A stress gradient creates a flux of atoms to the base of the surface grain. The accretion-induced shear stress has to overcome the grain boundary sliding friction, σ_{friction}. In the presence of an oxide layer, the accretion-induced shear stress must also crack the surface oxide (thickness, t, and strength τ), with $\sigma_{\text{oxide}} = \frac{2t}{a}\tau_{\text{oxide}}^{\text{fracture}}$, in order for grain boundary sliding to occur. The term $\Delta\sigma$ in Equation 1.4 is given by

$$\Delta\sigma = \sigma_m - \sigma_{\text{friction}}\frac{A_{\text{slide}}}{A_{\text{accum}}} - \sigma_{\text{oxide}} \tag{1.5}$$

Thus, a back stress in the whisker grain can be created, stopping the growth if the accretion-induced shear is not high enough for sliding. In summary, the critical factors in the growth rate analysis are σ_{friction}, the in-plane film average compressive stress

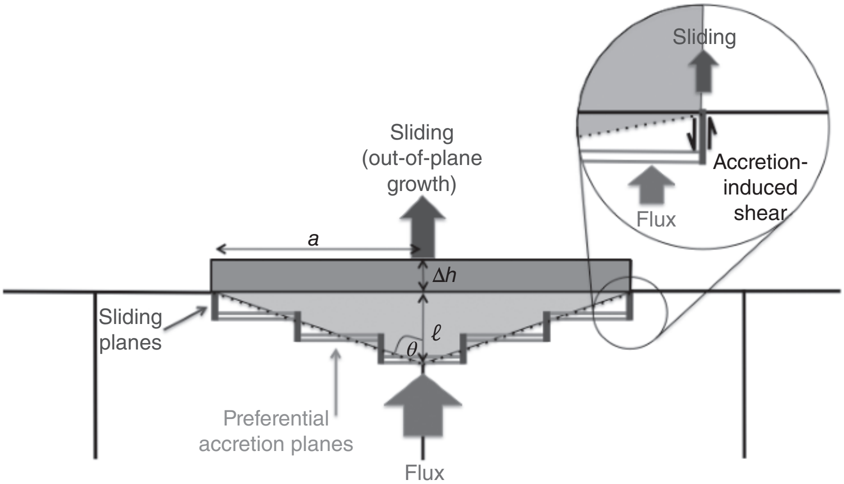

Figure 1.4 Schematics of a simple whisker growth model, delineating the roles of atomic accretion, faceting of the grain boundary (facets shown by vertical lines and horizontal double lines), and grain boundary sliding (along the sliding planes shown by vertical lines) on surface defect formation from a surface grain with ($0° < \theta < 90°$). Source: Reprinted with permission from Elsevier © 2013 [12].

σ_m, the stress required to produce a circumferential crack in the oxide of thickness t, and the surface grain geometry, a and θ. Thus, the steady-state growth rate of a surface grain as a whisker, with constant radius, derived from the two-dimensional continuity equation is

$$\frac{\Delta h}{\Delta t} = \left(\frac{\Omega D_{\text{eff}}}{RT \ln\left(\frac{b}{a}\right)} \right) \left(\frac{1}{a}\right) \left[\sigma_m - \left(\frac{1}{\tan\theta}\right) \sigma_{\text{friction}} - 2\left(\frac{t}{a}\right) \tau_{\text{oxide}}^{\text{fracture}} \right] \tag{1.6}$$

The implication of this steady-state growth model is that there exists a critical surface grain geometry for a given grain boundary sliding coefficient and oxide layer thickness, which determines if such a surface grain will grow out of plane via grain boundary sliding and Coble creep and, therefore, will become a whisker. Assuming that the effect of surface oxide thickness is relatively small, a normalized growth rate can be calculated as a function of surface grain depth and the $\sigma_{\text{friction}}/\sigma_m$ as shown in Figure 1.5.

The "No Growth" region in Figure 1.5 corresponds to the situation where the surface grain is deep (low θ) and the ratio between grain boundary sliding friction and the film stress ($\sigma_{\text{friction}}/\sigma_m$) is high. The "Growth" region in Figure 1.5 corresponds to the situation where the surface grain is shallow (θ approaches 90°) and the ratio between grain boundary sliding friction and the film stress ($\sigma_{\text{friction}}/\sigma_m$) is low. Cross sections of whisker grains consistently showed that the surface grains were shallow

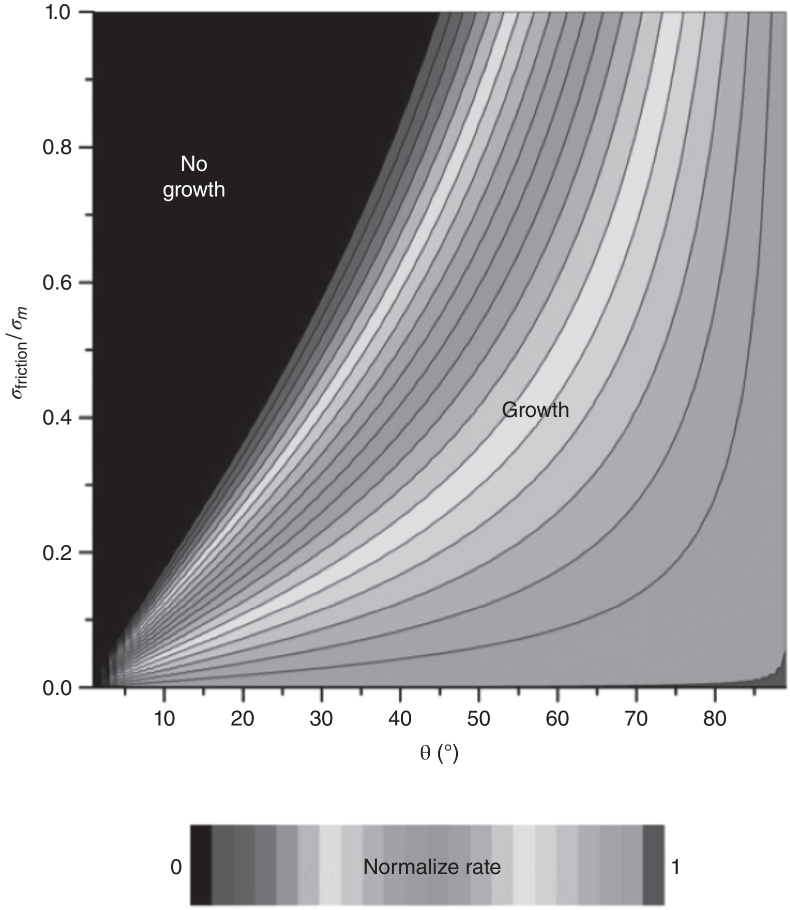

Figure 1.5 Effects of surface grain geometry and grain boundary sliding on whisker growth rate. The growth rate is normalized by the maximum growth rate and projected as a contour on the plot as a function of θ and $(\sigma_{\text{friction}}/\sigma_m)$. The critical θ_c for zero growth rate increases as the $(\sigma_{\text{friction}}/\sigma_m)$ increases, approaching 45° when $(\sigma_{\text{friction}}/\sigma_m) = 1$. The region of interest is $60° < \theta < 90°$, corresponding to those observed from cross sections of whiskers. Source: Reprinted with permission from Elsevier © 2013 [12]. Please visit www.wiley.com/go/Kato/TinWhiskerRisks to access the color version of this figure.

with $\theta > 60°$. Based on this model, long whiskers grow from shallow surface grains with easy grain boundary sliding in the direction of growth.

During growth by sliding limited creep without coupling between the shear stress and grain boundary migration, the grain boundaries forming the whisker root will remain stationary, resulting in a whisker with a constant diameter. In the case where growth is coupled with shear-induced grain boundary migration, the grain boundaries around a particular whisker may either move toward the center of the whisker, resulting in a whisker with a decreasing diameter and changing grain boundary curvatures to maintain the force balances at the interface junctions

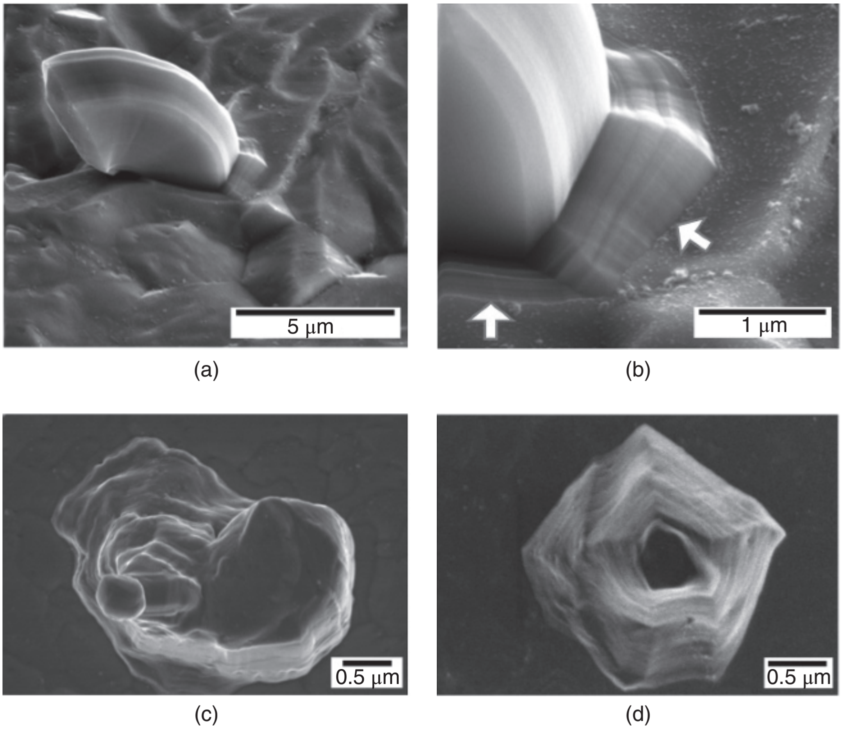

Figure 1.6 SEM images of (a) a whisker with a decreasing diameter as it grows, (b) higher magnification view of the base of the whisker shows the initial position of the surface grain (indicated by arrows) and surface striations corresponding to the positions of the grain boundary groove between the whisker and neighboring grain as it shrank, (c) whisker-to-hillock transition, and (d) hillock formation.

(Figs. 1.3 and 1.6a, b), or move away from the center of the whisker, resulting in a hillock (Fig. 1.6d) or whisker-to-hillock transition (Fig. 1.6c).

The occurrence of grain boundary migration and its directionality during whisker and hillock formation may be an indication of coupling between accretion-induced shear stress and grain boundary migration. The conditions and mechanisms for coupling migration and applied shear stresses are being elucidated through molecular dynamics (MD) and phase-field crystal simulations (PFC) [21, 22].

Cahn et al. [21] identified a wide range of processes that may result from coupling, including a transition between coupling modes that may lead to a stationary grain boundary and a “process that will look like grain boundary sliding.” They proposed that many phenomena, including diffusion-induced grain boundary migration (DIGM), may be caused by such coupling. Whisker morphologies such as the one shown in Figure 1.7 suggest that the lack of coupling between the accretion-induced shear stress and grain boundary migration may lead to the formation of long, straight whiskers, the ones more likely to cause short circuits in electronics.

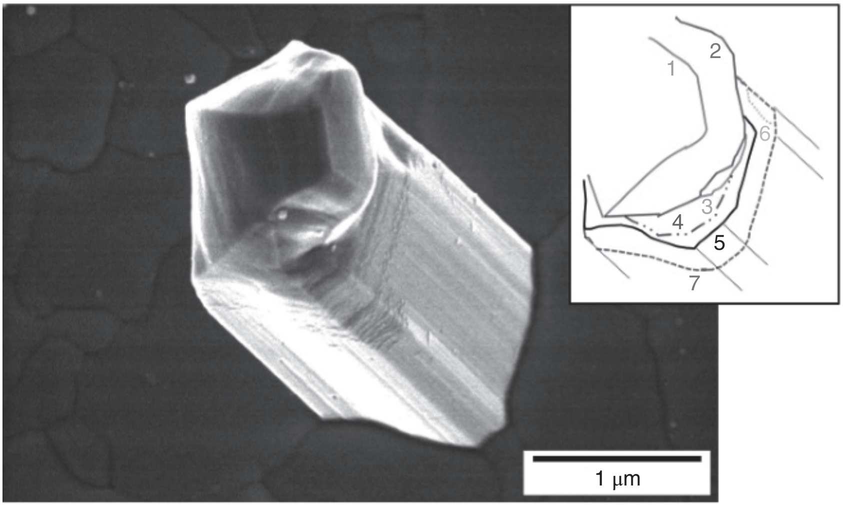

Figure 1.7 SEM image of a whisker growing on an electroplated Sn film, with the grain boundary contours (inset) of the whisker showing the changes in diameter and growth symmetry over time. Formation of a straight whisker seems to be associated with the cessation of grain boundary migration.

In Figure 1.7, the progression of grain boundary positions as the whisker grows can be seen starting from the tip of the whisker, where contour 1 corresponds to the original surface of the whisker. Contours 2 through 7 mark the positions of the grain boundaries between the whisker and its neighboring grains over time, with the whisker growing asymmetrically as it first increases, then decreases, and then increases in diameter.

Starting at approximately contour 6, the whisker grows with a close to constant profile, that is, the grain boundaries surrounding the whisker are no longer migrating as the whisker grows out of the film plane. Extensive, systematic MD and PFC studies of surface grains with different grain boundary orientations are needed to help us better understand the role of coupling and grain boundary sliding in whisker and hillock formation.

1.2.2 Whisker Formation and Fatigue Damage Accumulation during Thermal Cycling

The grain boundary sliding limited model for whisker growth explains whisker growth behavior not only during intermetallic growth at room temperature but also under thermal cycling conditions, where we have observed that the whisker radius changes with the number of thermal cycles [17].

Images of individual whiskers as a function of thermal cycling (−40 to 85°C) revealed that whiskers grew and their radii decreased, with a deep groove at the whisker roots, and eventually "pinched off." This whisker "pinch-off" process led to a decreasing whisker density with increasing number of thermal cycles.

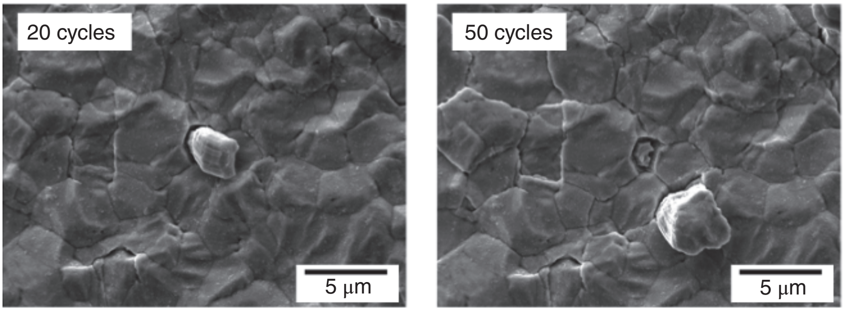

Figure 1.8 SEM images of a whisker at 20 and 50 cycles. The whisker on the left pinched off and disappeared between 20 and 50 cycles, leaving behind a remnant hole.

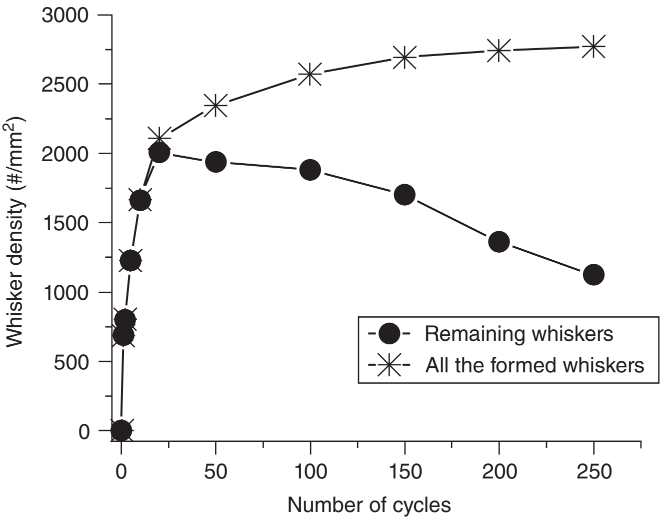

Figure 1.9 Whisker density as a function of number of thermal cycles: the circle symbol corresponds to the density of whiskers that remained on the sample surface; the star symbol corresponds to the density of all the formed whiskers, including those that disappeared after 20 cycles.

An example of this whisker "pinch-off" phenomenon is shown in Figure 1.8, where the whisker (with decreasing radius) disappeared between 20 and 50 thermal cycles and a new whisker started to grow. While the total number of whiskers (counting both the intact whiskers and the remaining holes of the whiskers that were "pinched off") increased with increasing thermal cycles, the rate of whisker "pinch-off" was much more rapid than the rate of whisker nucleation (Fig. 1.9).

The mechanistic model Wang et al. [17] proposed (as an extension to the model described earlier) for the pinch-off process is summarized in Figure 1.10.

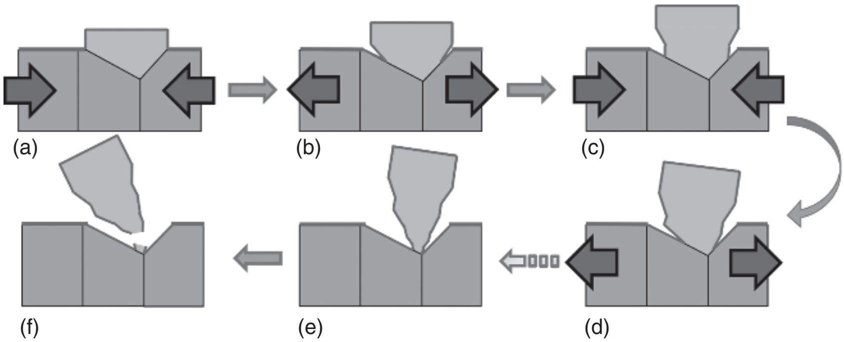

Figure 1.10 Schematic of the whisker pinch-off phenomenon. (a) Whisker grows due to a compressive stress upon heating; (b) during cooling, a crack forms at the whisker root due to the tensile stress; (c) subsequent heating leads to whisker growth with a smaller diameter; (d) crack propagates along whisker grain boundaries due to a tensile stress upon cooling; (e) whisker continues to grow with a further decreased diameter; and (f) when the whisker diameter is small enough, it becomes fragile enough to break off during handling. Source: Wang et al. [17].

Due to the coefficient of thermal expansion (CTE) mismatch between the Sn film and the Si substrate, the Sn film is under compression upon heating and under tension upon cooling. During the heating cycle, the whisker grows out of the film plane via grain boundary sliding to relieve the compressive stress. During the cooling cycle, tensile stress induces a crack at the whisker root. With the newly exposed Sn at the crack being oxidized, the crack cannot close when the tensile stress is removed and the growth during the next heating cycle leads to horizontal striation rings on the whisker surface. One horizontal striation ring corresponds to whisker growth during one thermal cycle [23].

With each subsequent heating and cooling cycle, the crack propagates down the oblique whisker grain boundaries, creating a deep groove at the whisker root, as seen in Figure 1.8. This groove causes a decrease in whisker radius with each thermal cycle, until the ever more fragile whiskers break off during routine handling of the films, that is, “pinch-off.” Striations are seen along both the whisker and the groove surfaces in the film that correspond to individual thermal cycles.

The implication of the “pinch-off” on the whisker growth rate is significant. As the whisker radius, a, decreases in the initial stage of the pinch-off process, the flux, J, to the base of the whisker increases, according to Equations 1.2 and 1.4. However, as the whisker diameter decreases, the growth of the whisker will, at some diameter, become kinetic-limited, either by diffusion along the whisker root or interface attachment.

As a decreases, grain boundary cracking and groove formation are often observed to be asymmetrical, with the whisker becoming completely detached from some neighboring grains. The resulting decrease in grain boundary area leads to an overall decrease in J. At this point, the whisker growth rate is better described by a one-dimensional continuity equation, where the stress gradient (i.e., the driving force for growth) and thus J decrease with decreasing a. The linearized stress gradient is given by

$$\nabla\sigma|_{x=a} = \left.\frac{\partial\sigma}{\partial x}\right|_{x=a} = \frac{\Delta\sigma}{3a_0 - a} \tag{1.7}$$

where a_0 is the original radius of the surface grain before the "pinch-off" process occurred.

In the case of a continuously reforming surface oxide, the accretion-induced shear stress may no longer be sufficient to break the oxide, which increases as a decreases, that is, $\sigma_{\text{oxide}} = 2(t/a)^{*}\tau_{\text{oxide}}$, such that

$$\sigma_m < \sigma_{\text{friction}}\frac{A_{\text{slide}}}{A_{\text{accum}}} + \sigma_{\text{oxide}} \tag{1.8}$$

Therefore, with increasing thermal cycles, the whisker growth rate initially increases and later decreases either until whisker "pinch-off" occurs or until growth stops when the accumulation-induced shear force is insufficient to overcome the grain boundary sliding friction or break the oxide.

Although the grain boundary sliding limited creep model provides some insights into the roles of grain geometry and grain boundary sliding in whisker growth, the microstructural selection process that predisposes some shallow surface grains to become whiskers and hillocks must be refined further. In the next section, the effects of grain boundary sliding friction and localized stress, which are highly dependent on grain boundary structure, grain orientations, and misorientations, are discussed.

1.2.3 Preferred Site Model Based on Crystallographic Misorientations as well as Elastic and Thermoelastic Anisotropic Properties

Besides the surface grain geometry and grain boundary sliding friction, there are several additional factors that predispose a particular surface grain to becoming a whisker. These factors include localization of high strain energy (the driving force for whisker formation) due to variation in local crystallographic orientations. Object-oriented finite element analysis (OOF) [24, 25] was utilized to examine the generation of local high ESEDs for the Sn grains with specific misorientations from the neighboring grains [26].

Grain orientations generated using the March–Dollase orientation distribution function [27, 28] for (001), (100), (110), and (111) fiber textures were randomly assigned to the grains in a two-dimensional, polycrystalline microstructure [where (hkl) planes of the grains are preferentially parallel to the film plane]. The plane stress condition ($\sigma_{zz} = \sigma_{xz} = \sigma_{yz} = 0$) was imposed to simplify the calculation for thin films. Elastic stresses induced at room temperature due to Cu_6Sn_5 IMC formation were generated assuming an in-plane biaxial compressive strain ($\varepsilon_1 = \varepsilon_2 = -0.01\%$) imposed on the films. For thermoelastic stresses during thermal cycling, the CTE mismatch between the Sn film and the Cu substrate was simulated by constraining the in-plane film strain to match the thermal expansion of the substrate for a

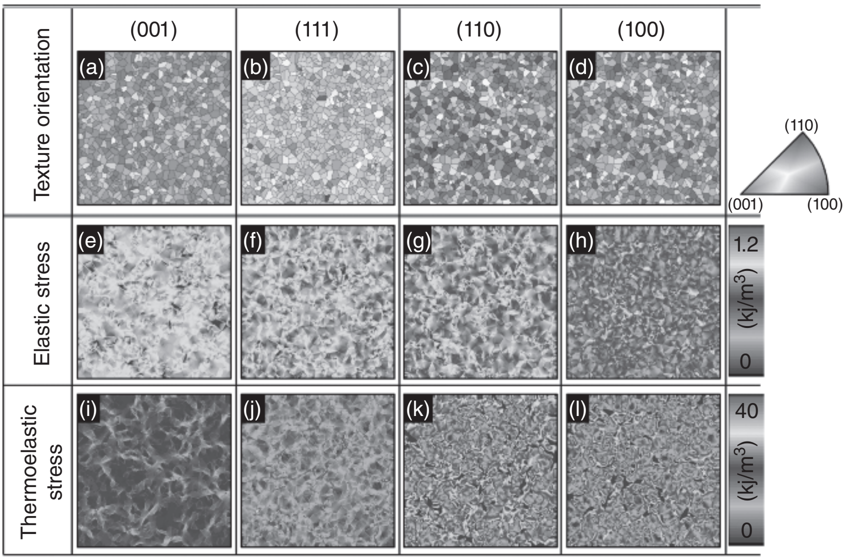

Figure 1.11 The grain orientation maps and simulated ESED distributions. (a)–(d) Normal direction grain orientation maps in inverse pole figure (IPF) colors for (001), (111), (110), and (100) textured films, respectively. The corresponding ESED distributions (e)–(h) for elastic stresses induced by room temperature aging due to IMC formation, and (i)–(l) for thermoelastic stresses induced during thermal cycling. ESED distributions for the same stress-generating mechanisms are scaled in the same manner. Please visit www.wiley.com/go/Kato/TinWhiskerRisks to access the color version of this figure.

temperature change from 25 to 85°C. The global and local responses to these stress conditions were analyzed in terms of ESEDs.

The global response varies significantly with the film texture, as shown in Figure 1.11. The textures for films with the lowest overall ESED are (100) textures for room temperature aging and (001) textures for thermal cycling conditions. In addition to the overall ESED for the entire film, locally high ESEDs associated with specific grain misorientations were observed and are shown in Figure 1.12.

These high ESED grains are identified as potential whiskers. The orientations of all the grains and those with high ESEDs (top 1%) are plotted using normal direction inverse pole figures (ND IPFs) in Figure 1.12.

For room temperature aging, (001) and (111) textured films have high ESED grains mostly orientated toward the (100). The orientations of high ESED grains evidently differ significantly from the primary texture. On the other hand, (110) textured films have most high ESED grains oriented toward the (110) and some oriented toward the (100), whereas (100) textured films have high ESED primarily grains oriented toward (100), identical to the primary texture.

For thermal cycling condition, (001) and (111) textured films have high ESED grains oriented between (110) and (100), far away from the texture, but the (110) and (100) textured films have high ESED grains with orientations similar to the textures.

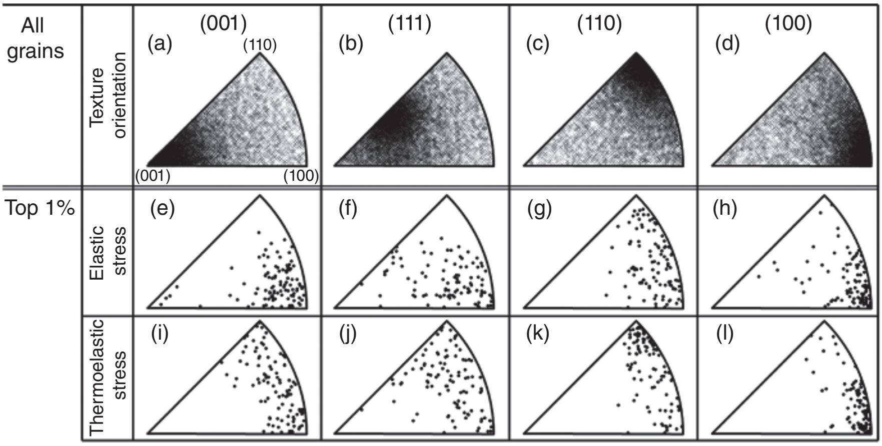

Figure 1.12 ND IPFs showing grain orientation distributions (a)–(d) for (001), (111), (110), and (100) textured films, respectively. Orientations of grains with high ESEDs (top 1%) for each texture are shown in ND IPFs (e)–(h) for elastic stresses and (i)–(l) for thermoelastic stresses. Each dot stands for one grain orientation.

In summary, the anisotropic elasticity (effective in-plane biaxial moduli) for room temperature aging and thermoelasticity (CTE mismatch or thermal cycling) caused nonuniform, highly localized ESEDs. These high ESED grains commonly have their c-axes aligned with the film plane but also depend on the textures and stress conditions. Thus, further analysis must take into account all the directions in orientation space (ND and in-plane directions), as well as the anisotropic elastic and thermoelastic properties of β-Sn.

For the case of a film with a (111) texture, the local elastic strains have been measured and compared to the simulation results for the room temperature aging condition. Local grain orientations, deviatoric elastic strains, and ESEDs have been measured using synchrotron microdiffraction in regions containing whiskers or hillocks for films, whose primary texture is near (111) [11].

An example of the comparison is shown in Figure 1.13: a secondary electron microscopy (SEM) image of a scanned area around a whisker (Fig. 1.13a), the orientations of the whisker grain (811) and the other grains in the film projected in normal direction (ND) inverse pole figure (IPF) (Fig. 1.13b), the corresponding microdiffraction (Fig. 1.13c), and simulated (Fig. 1.13d) grain orientation maps, measured out-of-plane elastic strain (Fig. 1.13e) and ESED distribution maps (Fig. 1.13g), as well as simulated out-of-plane elastic strain (Fig. 1.13f) and ESED distribution (Fig. 1.13h) maps. Similarly for two other whiskers and six hillocks in the room temperature aging condition, the whisker/hillock grain orientations differ significantly from the film textures.

The three whisker and six hillock grains were observed to have higher crystallographic misorientations with neighboring grains (average peak misorientation angle of 65° for whiskers and 80° for hillocks) than generally observed in the

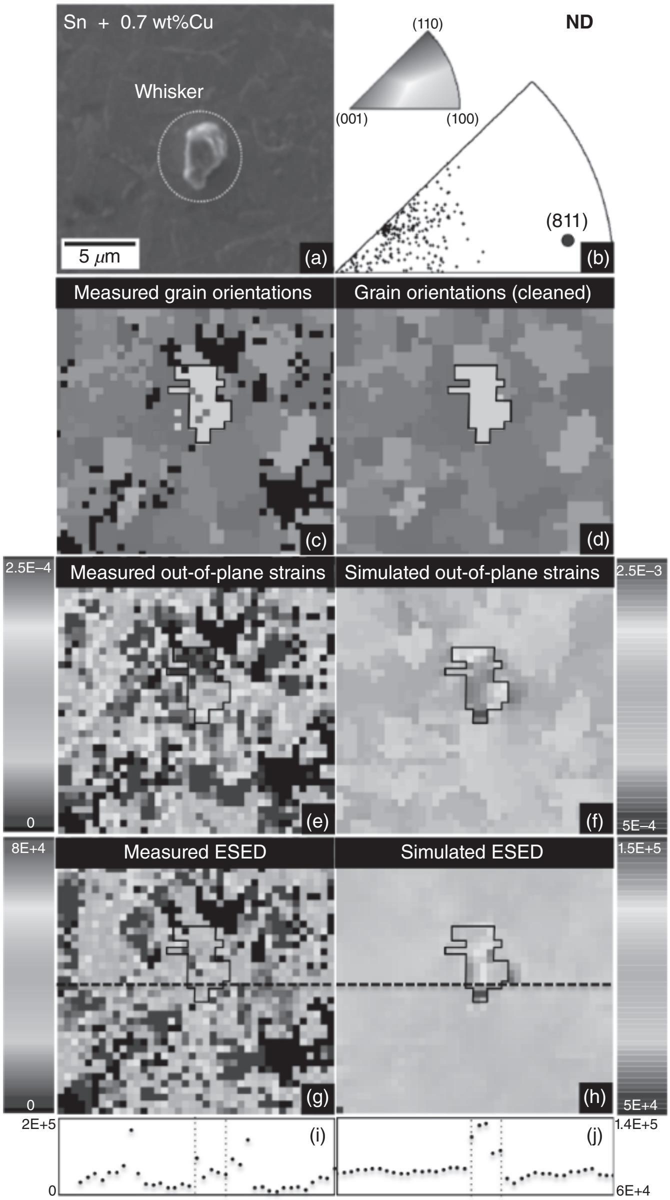

Figure 1.13 (a) SEM image of a whisker on Sn + 0.7 wt%Cu film. (b) Orientation of the whisker grain (pink), (811), and other grains in the film (black) displayed in ND equal-area IPF. (c) As-collected grain map in normal direction inverse pole figure colors. (d) Cleaned grain map in ND IPF colors. (e) Measured out-of-plane strain distribution from microdiffraction. (f) OOF-simulated out-of-plane strain distribution. (g) Measured ESED distribution. (h) OOF-simulated ESED distribution. (i) and (j) are line plots of measured and simulated ESED as a function of distance across the whisker grain corresponding to the position of the dashed line in (g) and (h). Source: Reprinted with permission from Cambridge University Press © 2013 [11]. Please visit www.wiley.com/go/Kato/TinWhiskerRisks to access the color version of this figure.

microstructure (average peak misorientation angle of 50° for randomly selected grain pairs). While elastic simulations predicted higher local out-of-plane elastic strains and ESEDs for whisker and hillock grains, synchrotron measurements of out-of-plane strains of whisker and hillock grains after growth showed relaxation, with correspondingly low ESEDs calculated from measured strains.

This comparison suggests that, before whisker or hillock formation, highly misoriented grains with high out-of-plane elastic strains and ESEDs relative to their neighbors determined, at least in part, which grains became whiskers or hillocks. Due to the highly anisotropic properties of β-Sn, the local grain orientations as well as misorientations determine grains with high ESEDs, in response to external strains (due to IMC formation or temperature changes).

The combined results from simulation and experiment verify that grains with high ESEDs are potential whisker formation sites. Extending this to the overall microstructure and to the films, we have identified whisker-resistant textures (low ESEDs) under different stress-generating mechanisms: a strong (100) fiber texture film for a compressive stress induced only by IMC formation and a strong (001) fiber texture film for a compressive stress induced during thermal cycling.

1.3 SUMMARY AND RECOMMENDATIONS

In this chapter, we examined the characteristic properties of the microstructure around whisker and hillock grains with the aim to further identify why these particular shallow surface grains and locations became predisposed to forming whiskers and hillocks.

On the local level, three major factors play a role in determining which surface grains will become a whisker/hillock, including the surface grain geometry, crystallographic orientation-dependent surface grain boundary structure, and the localization of elastic strain/strain energy density distribution due to variation in crystallographic orientations and β-Sn anisotropy.

A growth model was developed, based on grain boundary faceting, localized Coble creep, and grain boundary sliding for whiskers. In this model of whisker formation, two mechanisms are important: accretion of atoms by Coble creep on grain boundary planes normal to the growth direction inducing a grain boundary shear and grain boundary sliding in the direction of whisker growth.

The model accurately captures the importance of the geometry of surface grains – shallow grains on film surfaces whose depths are significantly less than their in-plane grain sizes. On the basis of this model, long whiskers grow from shallow surface grains with easy grain boundary sliding in the direction of growth.

For the thermal cycling condition, a whisker “pinch-off” phenomenon was observed, where the whisker radius decreases as growth occurs. The decrease in whisker radius resulted in the initial increase in the flux (and thus the growth rate), followed by the decrease in stress gradient and increase in resistance to oxide breaking, resulting in reduced growth rate.

Local grain orientations and strains measured by synchrotron microdiffraction in regions containing whiskers or hillocks were compared with elastic finite element analysis simulations. Whisker and hillock grains were observed to have higher crystallographic misorientations with neighboring grains than generally observed in the microstructure.

While elastic simulations predicted higher local out-of-plane elastic strains and ESEDs for whisker and hillock grains, synchrotron measurements of out-of-plane strains of whisker and hillock grains after growth showed relaxation, with correspondingly low ESEDs calculated from measured strains. This suggests that, before whisker or hillock formation, highly misoriented grains with high out-of-plane elastic strains and ESEDs relative to their neighbors determined, at least in part, which grains became whiskers or hillocks.

These two-dimensional simulations of film response to strains imposed by two different aging conditions – room temperature and thermal cycling – may therefore be a useful method for evaluating and predicting the propensity of a film with a particular texture to form whiskers. Hence, it may be possible to engineer a whisker-resistant texture for the appropriate aging condition. Furthermore, while complete elimination of surface grains may be impossible, the combination of a whisker-resistant texture and a uniformly high grain boundary sliding coefficient may serve to significantly reduce the risk of whisker formation.

ACKNOWLEDGMENTS

The authors gratefully acknowledge support from NSF Graduate Research Fellowship Program, Cisco Systems, Inc., Foresite Inc., Army Research Laboratories, and Naval Surface Warfare Center (Crane Division). We would like to thank Dr Peng Su, Maureen Williams, Dr Anthony Rollett, Dr Martin Kunz, and Dr Nobumichi Tamura for assistance with data extraction and valuable discussions.

We acknowledge support from DOE-BES (DE-FG02-05ER15637) and NSF (EAR-0337006) and access to ALS beamline 12.3.2. ALS is supported by the Director, Office of Science, Office of Basic Energy Sciences, Materials Science Division, of the US Department of Energy under Contract no. DE-AC02-05CH11231. The microdiffraction program at the ALS beamline 12.3.2 was made possible by NSF grant # 0416243.

Sandia National Laboratories is a multiprogram laboratory managed and operated by Sandia Corporation, a wholly owned subsidiary of Lockheed Martin Corporation, for the US Department of Energy's National Nuclear Security Administration under contract DE-AC04-94AL85000.

This chapter is reproduced from Springer Journal of Metals, A Predictive Model for Whisker Formation Based on Local Microstructure and Grain Boundary Properties, 65 [10] (2013) 1350–1361, P. Sarobol, Y. Wang, W. H. Chen, A.E. Pedigo, J.P. Koppes, J.E. Blendell, and C.A. Handwerker, published online August 24, 2013, with kind permission of Springer Science+Business Media.

REFERENCES

1. Sobiech M, Welzel U, Mittemeijer EJ, Hügel W, Seekamp A. Driving force for Sn whisker growth in the system Cu–Sn. Appl Phys Lett 2008;93:011906.
2. Sobiech M, Wohlschlögel M, Welzel U, Mittemeijer EJ, Hügel W, Seekamp A, Liu W, Ice GE. Local, submicron, strain gradients as the cause of Sn whisker growth. Appl Phys Lett 2009;94:221901.
3. Tu KN. Irreversible processes of spontaneous whisker growth in bimetallic Cu–Sn thin-film reactions. Phys Rev B 1994;49:2030.
4. Lee BZ, Lee DN. Spontaneous growth mechanism of tin whiskers. Acta Mater 1998;46:3701.
5. Chason E, Jadhav N, Chan WL, Reinbold L, Kumar KS. Whisker formation in Sn and Pb–Sn costings: role of intermetallic growth, stress evolution and plastic deformation process. Appl Phys Lett 2008;92:171901.
6. Kumar KS, Reinbold L, Bower A, Chason E. Plastic deformation processes in Cu/Sn bimetallic films. J Mater Res 2008;23:2916.
7. Boettinger WJ, Johnson CE, Bendersky LA, Moon K-W, Williams ME, Stafford GR. Whisker and Hillock formation on Sn, Sn–Cu and Sn–Pb electrodeposits. Acta Mater 2005;53:5033.
8. Pei F, Jadhav N, Chason E. Correlation between surface morphology evolution and grain structure: Whisker/hillock formation in Sn–Cu. JOM 2012;64:1176.
9. Moon KW, Johnson CE, Williams ME, Kongstein O, Stafford GR, Handwerker CA, Boettinger WJ. Observed correlation of Sn oxide film to Sn whisker growth in Sn–Cu electrodeposit for Pb-free solders. J Electron Mater 2005;34:L31.
10. Jadhav N, Buchovecky E, Chason E, Bower A. Real-time SEM/FIB studies of whisker growth and surface modification. JOM 2010;62:30.
11. Sarobol P, Chen WH, Pedigo AE, Su P, Blendell JE, Handwerker CA. Effects of local grain misorientation and beta-Sn elastic anisotropy on whisker and hillock formation. J Mater Res 2013;28:747.
12. Sarobol P, Blendell JE, Handwerker CA. Whisker and hillock growth via coupled localized Coble creep, grain boundary sliding, and shear induced grain boundary migration. Acta Mater 2013;61:1991.
13. Frolov T, Boettinger WJ, Mishin Y. Atomistic simulation of hillock growth. Acta Mater 2010;58:5471.
14. Pei F, Jadhav N, Chason E. Correlating whisker growth and grain structure on Sn–Cu samples by real-time scanning electron microscopy and backscattering diffraction characterization. Appl Phys Lett 2012;100:221902.
15. Galyon GT, Palmer L. An integrated theory of whisker formation: the physical metallurgy of whisker formation and the role of internal stresses. IEEE Trans Electron Packag Manuf 2005;28:17.
16. Vianco PT, Rejent JA. Dynamic recrystallization (DRX) as the mechanism for Sn whisker development. Part I: A model. J Electron Mater 2009;38:1815–1825.
17. Wang Y, Blendell JE, Handwerker CA. Evolution of tin whiskers and subsiding grains in thermal cycling. J Mater Sci 2014;49:1099–1113.
18. Sarobol P, Koppes JP, Chen WH, Su P, Blendell JE, Handwerker CA. Recrystallization as a nucleation mechanism for whiskers and hillocks on thermally cycled Sn-alloy solder films. Mater Lett 2013;99:76.

19. Koppes JP, Ph.D. Thesis, Purdue University: West Lafayette, IN; 2012.
20. Pedigo AE, Handwerker CA, Blendell JE, Proceedings of the Electronic Components and Technology Conference; Lake Buena Vista, Florida, USA: IEEE; 2008. p 1498.
21. Cahn JW, Mishin Y, Suzuki A. Coupling grain boundary motion to shear deformation. Acta Mater 2006;54:4953.
22. Trautt ZT, Adland A, Karma A, Mishin Y. Coupled motion of asymmetrical tilt grain boundaries: molecular dynamics and phase field crystal simulations. Acta Mater 2012;60:6528.
23. Suganuma K, Baated A, Kim K-S, Hamasaki K, Nemoto N, Nakagawa T, Yamada T. Sn whisker growth during thermal cycling. Acta Mater 2011;59:7255.
24. Langer SA, Fuller E, Carter WC. OOF: an image-based finite-element analysis of material microstructures. Comput Sci Eng 2001;3:15.
25. Reid ACE, Lua RC, García RE, Coffman VR, Langer SA. Modelling microstructures with OOF2. Int J Mater Prod Technol 2009;35:361.
26. Chen WH, Sarobol P, Holaday J, Handwerker CA, Blendell JE. Effect of crystallographic texture, anisotropic elasticity and thermal expansion on whisker formation in β-Sn thin films. J Mater Res 2014;29:197–206.
27. Blendell JE, Vaudin MD, Fuller ER. Determination of texture from individual grain orientation measurements. J Am Ceram Soc 1999;82:3217.
28. Dollase WA. Correction of intensities for preferred orientation in powder diffractometry: application of the March model. J Appl Crystallogr 1986;19:267.